



Trans. Nonferrous Met. Soc. China 32(2022) 696-708

Transactions of Nonferrous Metals Society of China

www.tnmsc.cn



Thermodynamic modeling of ZrO₂–CaO–TiO₂ system

Shi-yu HE^{1,2}, Qi-sheng FENG^{1,2}, Bao-hua DUAN^{1,2}, Guang-yao CHEN^{1,2}, Zhu WU³, Chong-he LI^{1,2}, Xiong-gang LU^{1,2,4}

- 1. State Key Laboratory of Advanced Special Steel, Shanghai Key Laboratory of Advanced Ferrometallurgy, School of Materials Science and Engineering, Shanghai University, Shanghai 200444, China;
 - 2. Shanghai Special Casting Engineering Technology Research Center, Shanghai 201605, China;
 - 3. Shanghai Institute of Microsystem and Information Technology, Chinese Academy of Sciences, Shanghai 201800, China;
 - 4. School of Materials Science, Shanghai Dianji University, Shanghai 201306, China

Received 27 January 2021; accepted 10 September 2021

Abstract: The phase diagram of ZrO₂–CaO–TiO₂ system was essential for the development of photocatalytic materials and refractory materials. In this work, the ZrO₂–CaO–TiO₂ system was accessed by using the CALPHAD method. The substitutional solution models were used to describe liquid and solid solution phases, the sub-lattice models were used to describe ternary compounds, and then the thermodynamic parameters were obtained by the least square method combined with literature experiment results. The acquired thermodynamic parameters were used to calculate the isothermal sections of the ZrO₂–CaO–TiO₂ system at 1473 and 1673 K. There existed a good agreement between experimental and predicted phase relationships, the experimental points which were inconsistent with calculated results may be attributed to experimental errors and the sluggish kinetics of cations for ZrO₂-based materials. In order to further verify the validity of the database, the thermodynamic parameters were also used to simulate the thermodynamic properties (specific heat capacity, enthalpy, and entropy) of CaZrTi₂O₇ within 5% errors. Good consistency demonstrated that the present thermodynamic database was self-consistent and credible.

Key words: ZrO₂-CaO-TiO₂ system; Gibbs free energy model; CALPHAD method; isothermal sections

1 Introduction

Ceramic materials based on the ZrO₂ have been extensively applied in many industrial fields including basic conductive elements of single crystal [1], photocatalytic material [2], positive temperature coefficient thermistor, and refractory materials [3,4]. For example, the photocatalytic materials based on TiO₂ can acquire a higher surface area as well as a higher thermal and mechanical stability by dropping second components such as CaO and ZrO₂ [5], while the

stability of c-ZrO₂ (cubic) structure can be improved by adding some CaO and TiO₂ [6]. To understand the preparation and properties of these materials, a reliable phase diagram of ZrO₂–CaO–TiO₂ system is absolutely necessary.

This ternary system includes three binary systems ZrO₂–CaO, ZrO₂–TiO₂, and TiO₂–CaO. Among them, the ZrO₂–CaO [7] and ZrO₂–TiO₂ [8] systems were re-assessed by our group, and another phase diagram of TiO₂–CaO system was studied by UMEZU [9], DEVRIES et al [10], and ROTH [11]. Recently, GONG et al [12] have systematically calculated TiO₂–CaO system by using the CALPHAD

method [13], and the results were considered in the present work. The calculated phase diagrams of ZrO₂-CaO-TiO₂ system have not been reported completely, but some experimental phase equilibria have been carried out by SWENSON et al [1], COUGHANOUR and ROTH [14], FIGUEIREDO et al [15], and PREDA et al [16]. The phase equilibria of ZrO₂-CaO-TiO₂ system were firstly studied by COUGHANOUR and ROTH [14], who focused on the stoichiometric compound zirconolite (CaZrTi₂O₇) and its phase relationships 1723-1823 K. ROSSELL [17] pointed out that the zirconolite formula of was identified $CaZr_xTi_{3-x}O_7$ (x was 0.833-1.25 at 1473 K, and 0.968-1.364 at 1673 K). Another ternary phase calzirtite (Ca₂Zr₅Ti₂O₁₆) was firstly detected by PYATENKO and PUDOVKINA [18]. This ternary phase also possessed a homogeneity range between Zr and Ti. Then, SWENSON et al [1] completely measured the isothermal sections of ZrO2-CaO-TiO₂ system at 1473 K by prolonging the time of heat treatment. Although the samples in their work underwent a protracted solution treatment, it was hard to reach equilibrium for phase reactions on the ZrO₂-rich side due to the sluggish kinetics of cations [19].

Thus, our present work aimed to establish a set of compatible and reliable phase diagrams of the ZrO₂–CaO–TiO₂ system using the CALPHAD method coupled with experimental information, which is particularly relevant to current preparation and operating conditions for high-temperature materials.

2 Literature review

2.1 Binary system

As shown in Fig. 1 and Fig. 2, The phase diagrams of ZrO₂–CaO [7] system and ZrO₂–TiO₂ [8] systems were re-optimized by our group using the CALPHAD technology. The substitutional solution models were used to simulate solid solution and liquid phases, the atomic sub-lattice models were used to simulate compounds, and the calculated results were in agreement with most evaluative conclusions. Thus, their thermodynamic parameters for the ZrO₂–TiO₂ and ZrO₂–CaO systems were directly adopted in this work.

The phase diagram of TiO₂-CaO system (Fig. 3) has been widely studied in the field of electronic

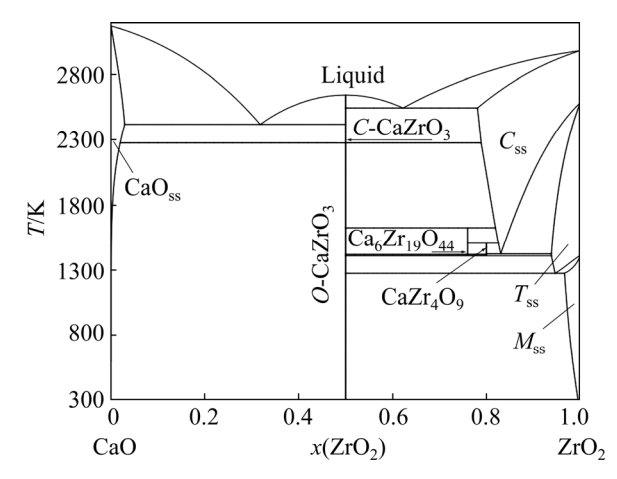


Fig. 1 Calculated phase diagram of ZrO_2 –CaO system in previous work [7] (C_{ss} , T_{ss} and M_{ss} represent cubic, tetragonal and monoclinic phases, respectively)

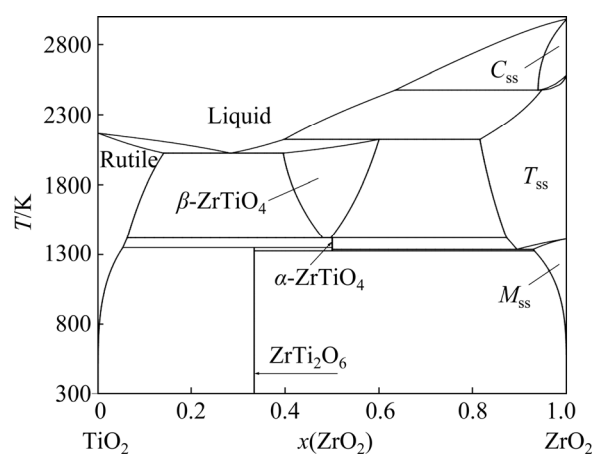


Fig. 2 Calculated phase diagram of ZrO₂-TiO₂ system in previous work [8]

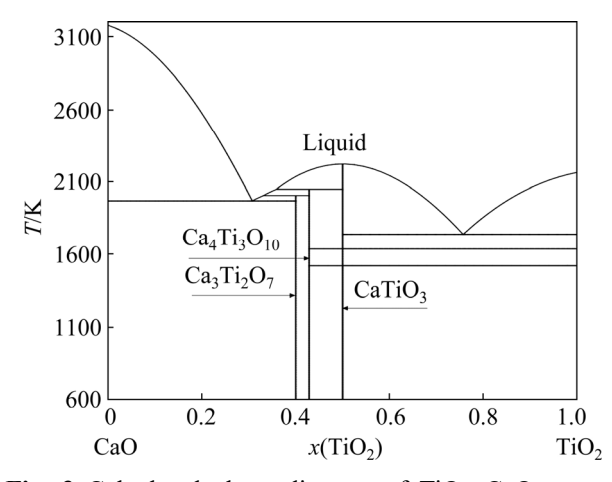


Fig. 3 Calculated phase diagram of TiO₂-CaO system according to Ref. [12]

industry because of its excellent electronic properties [12]. The early studies began in 1930

when UMEZU [9] discovered the phase equilibrium relationships in the TiO2-rich corner. The results implied the existence of CaTiO₃, Ca₃Ti₂O₇ and Ca₂TiO₄ intermediate compounds by the X-ray diffraction principle. Then, DEVRIES et al [10] and ROTH [11] systematically evaluated the phase equilibrium relationships through a series of precise experiments. It is worth mentioning that the Ca₄Ti₃O₁₀ compound was firstly discovered by ROTH [11]. The samples with a Ca/Ti molar ratio of 4:3 were synthesized by solid-phase sintering technology. Besides, using the CALPHAD method, KAUFMAN [20], KIRSCHEN and DECAPITANI [21], and DANĚK and NERÁD [22] determined the phase diagram of TiO2-CaO system based on thermodynamic models and experimental data; whereas, KIRSCHEN and DECAPITANI [21] and DANĚK and NEKAD [22] replaced Ca₄Ti₃O₁₀ with Ca₅Ti₄O₁₃, which was different from the work of KAUFMAN [20]. To solve this difference, GONG et al [12] proved the nonexistence of Ca₅Ti₄O₁₃ in the diagram of the TiO₂-CaO system using the XRD method. Based on the results, the phase diagram TiO₂-CaO of system re-optimized by GONG et al [12] with the CALPHAD method. In their work, CaTiO₃ was classified as three types of structures containing orthorhombic, tetragonal, and cubic structures, where the orthorhombic structure transformed to the tetragonal structure at about 1512 K, and the tetragonal structure transformed to cubic structure at about 1635 K. The calculation results from GONG et al [12] were considered in this work.

2.2 ZrO₂-CaO-TiO₂ system

2.2.1 Phase equilibria in ZrO₂-CaO-TiO₂ system

According to previous literature, there were several publications for the phase diagram of ZrO_2 –CaO– TiO_2 system. In 1955, the phase relationships of ZrO_2 –CaO– TiO_2 system at 1723–1823 K were studied by COUGHANOUR and ROTH [14] using X-ray diffraction analytical techniques. Their research focused on the phase equilibrium relationships in the ZrO_2 -rich and TiO_2 -rich areas. For the ZrO_2 -rich corner, the compounds $CaTiO_3$ and $CaZrO_3$ extended to the regions of $ZrO_2(C_{ss})$ and $ZrO_2(T_{ss})$, leading to a ternary phase region. For the TiO_2 -rich corner, there were two ternary phase areas including $(TiO_2 + CaZrTi_2O_7 + CaTiO_3)$ and $(TiO_2 + CaZrTi_2O_7 + CaTiO_3)$ and $(TiO_2 + CaZrTi_2O_7 + CaTiO_3)$

TiZrO₄). Additionally, it was also proposed by COUGHANOUR and ROTH [14] that the perovskite phases of CaTiO₃ and CaZrO₃ could form a series of continuous solid solutions.

FIGUEIREDO et al [15] measured the phase equilibria in the ZrO₂–CaO–TiO₂ system along the "zirconolite" (CaZrTi₂O₇) line at 1573 K by utilizing X-ray diffraction techniques. The samples were synthesized in air up to 1470 K for 24 h and to 1517 K for 12 and 60 h by solid sintering technology. However, the phase boundary line "zirconolite–CaZrO₃" intersected with another line "calzirtite–CaTiO₃", which violated the rule of phase relationships.

As shown in Fig. 4, the phase equilibria of ZrO₂–CaO–TiO₂ system at 1473 K were studied by SWENSON et al [1] applying X-ray diffraction and electron probe microanalysis techniques for the first time. However, their experiments involved the phenomenon of thermodynamic nonequilibrium, which reduced the accuracy of measurement results.

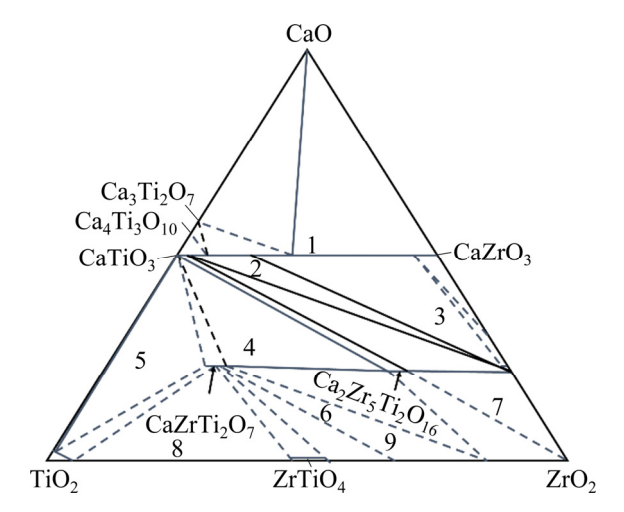


Fig. 4 Phase equilibria in ZrO₂–CaO–TiO₂ system at 1473 K (Figure reprinted with permission from Ref. [1])

The following year, PREDA et al [16] reported the isothermal section of ZrO_2 –CaO– TiO_2 system in the temperature range of 1623–1723 K by detecting a large number of samples with X-ray diffraction technique. However, samples were only thermally treated at 1623–1723 K for 2 h. The holding time was too short to reach dynamic equilibrium, especially for the transition from M_{ss} to T_{ss} . Thus, experimental results of PREDA et al [16] may not be credible.

The phase relationships in the ZrO_2 -CaO- TiO_2 system caused some debates on the ZrO_2 -rich

corner due to the slow dynamics. Thus, it is necessary to establish a set of reliable phase diagrams at different temperatures by combining theory with experiments based on the CALPHAD method.

2.2.2 Ternary phase

Up to now, two ternary phases (CaZrTi₂O₇ and Ca₂Zr₅Ti₂O₁₆) in the ZrO₂-CaO-TiO₂ system have been reported. The zirconolite (CaZrTi₂O₇) has been studied by many researchers because of its application in the design of high-level radioactive waste and immobilization of refractory ceramics [23]. In 1955, COUGHANOUR and ROTH [14] reported the existence of zirconolite by using X-ray diffraction for the first time. The structure of zirconolite was reported by ROSSELL [17], who described the crystal structure as a monoclinic distorted, anion-deficient, and fluorite-related superstructure. Furthermore, he found that zirconolite possessed an obvious small composition range between TiO2 and ZrO2, and its formula was considered as CaZr_xTi_{3-x}O₇, where the values of x were from 0.833 to 1.25 at 1573 K and from 0.968 to 1.364 at 1753 K. Subsequently, the range of chemical formula CaZr_xTi_{3-x}O₇ was remeasured by SWENSON et al [1], and the values of x are in the range of 0.836-1.157 at 1473 K, which were smaller than that of ROSSELL [17] at 1573 K. In the work of VANCE et al [23], the thermal expansion effects of hot-pressed CaZrTi₂O₇ in the temperature range of 1473-1773 K were reported using high-temperature X-ray diffraction and differential thermal analysis. The results indicated that CaZrTi₂O₇ did not undergo any phase change below 1723 K.

There were limited publications about Ca₂Zr₅Ti₂O₁₆ in the ZrO₂–CaO–TiO₂ system. PYATENKO and PUDOVKINA [18] discovered the ternary phase Ca₂Zr₅Ti₂O₁₆ by X-ray diffraction technology and proposed an anion-deficient fluorite-related superstructure with ideal fluorite-derived atomic coordinates. Subsequently, the structure of Ca₂Zr₅Ti₂O₁₆ was determined as tetragonal one by ROSSELL [17] using electron and X-ray diffraction patterns. Based on the description of ROSSELL [17], calzirtite belongs to the space lattice group *I*4~/*acd* with the parameters *a*=15.2203 Å, and *c*=10.1224 Å. In addition, SWENSON et al [1] reported a rather narrow range

between TiO_2 and ZrO_2 in the calzirtite with the chemical formula $Ca_2Zr_{7-x}Ti_xO_{16}$, where the value of x was 1.564–2.112 at 1473 K.

Due to the complex solid solution mechanism, the zirconolite and calzirtite were described as sublattice models, Ca(Zr,Ti)(Ti,Zr)₂O₇ and Ca₂(Zr,Ti)₅-(Zr,Ti)₂O₁₆ in the present work. In view of the reasonable experimental phase diagram from SWENSON et al [1] at 1473 K, their experimental data were used for optimizing the zirconolite and calzirtite.

3 Thermodynamic modeling

In the present work, the Gibbs free energies of pure unary components were given by

$$G_i^{0,\varnothing} = a + bT + cT \ln T + dT^2 + eT^3 + f/T + \sum_n g_n T^n$$
(1)

where $G_i^{0,\varnothing}$ is the Gibbs free energy of pure component i in \varnothing , T is the thermodynamic temperature, the items a to f and g_n are coefficients, and n stands for a set of integers.

Intermediate compounds such as $Ca_3Ti_2O_7$, $Ca_4Ti_3O_{10}$ were described as stoichiometric compounds. Their Gibbs free energies are given by

$$G = \sum_{i=1}^{n} x_i G_i^{0,\emptyset} + a + bT$$
 (2)

where $G_i^{0,\mathcal{O}}$ represents the Gibbs free energy of pure oxides (TiO₂, CaO, or ZrO₂) which are the basis of complex oxides, x_i is the molar fraction of a simple component i, a and b are the thermodynamic parameters, which need to be optimized in the present work.

The ultimate objective of the present work is to design new refractories for melting high-performance titanium alloy. It is necessary to study the interface reactions between the refractory and the titanium melt, but the ion sublattice model is not suitable for simulating the titanium melt. Therefore, the atomic sublattice model was selected for present optimization. In this work, the liquid and solid solution phases were described by the substitutional solution model. The Gibbs free energies of all these solutions are given by

$$G^{\varnothing} = \sum_{i=1}^{n} x_i G_i^{0,\varnothing} + RT \sum_{i=1}^{n} x_i \ln x_i + G^{\text{ex},\varnothing}$$
(3)

where R is the molar gas constant, and $G^{\text{ex},\emptyset}$ is the excess Gibbs energy of phase, which is defined as

$$G^{\text{ex},\emptyset} = \sum_{i,j=1(i\neq j)}^{n} x_i x_j \sum_{i,j=1(i\neq j)}^{n} L_{(i,j)}^{k} (x_i - x_j)^{k} + \sum_{i,j,l=1(i\neq j)}^{n} x_i x_j x_l \sum_{k} L_k V_k$$
(4)

where x_i , x_j and x_l are molar fractions of compounds i, j and l, respectively, the first term represents the binary interaction, and the second one stands for the ternary interaction. $L_{(i,j)}^k$ is the binary interaction parameter for the i-j binary, L_k is the ternary interaction parameter, and V_k is defined as

$$V_{k} = x_{k} + \left(1 - \sum_{p=i,j,l} x_{p}\right) / n \tag{5}$$

where x_k and x_p are the molar fractions of components k and p, respectively.

There is a homogeneity range between Zr and Ti in CaZrTi₂O₇, Ca₂Zr₅Ti₂O₁₆, CaTiO₃, CaZr₄O₉, and CaZrO₃. Thus, CaTiO₃, CaZr₄O₉, and CaZrO₃ are described as double sub-lattice models with $(CaO)_{1/(x+1)}(ZrO_2,TiO_2)_{x/(x+1)}$ (x=1,4). CaZrTi₂O₇ and Ca₂Zr₅Ti₂O₁₆ are described as three sub-lattice models with $(CaO)_{0.25}(ZrO_2,TiO_2)_{0.25}(TiO_2,ZrO_2)_{0.5}$ and $(CaO)_{0.222}(ZrO_2,TiO_2)_{0.556}(TiO_2,ZrO_2)_{0.222}$, respectively. The Gibbs free energy of zirconolite (*G*) can be given by

$$G = y_{\text{CaO}}^{1} y_{\text{TiO}_{2}}^{2} y_{\text{ZrO}_{2}}^{3} G_{\text{CaO:TiO}_{2}:\text{ZrO}_{2}}^{0} + y_{\text{CaO}}^{1} y_{\text{TiO}_{2}}^{2} y_{\text{TiO}_{2}}^{3} G_{\text{CaO:TiO}_{2}:\text{ZrO}_{2}}^{0} + y_{\text{CaO}}^{1} y_{\text{ZrO}_{2}}^{2} y_{\text{TiO}_{2}}^{3} G_{\text{CaO:TiO}_{2}:\text{ZrO}_{2}}^{0} + y_{\text{CaO}}^{1} y_{\text{ZrO}_{2}}^{2} y_{\text{TiO}_{2}}^{3} G_{\text{CaO:TiO}_{2}:\text{ZrO}_{2}}^{0} + y_{\text{CaO}}^{1} y_{\text{ZrO}_{2}}^{2} y_{\text{ZrO}_{2}}^{3} G_{\text{CaO:TiO}_{2}:\text{ZrO}_{2}}^{0} + RT[0.25 \left(y_{\text{TiO}_{2}}^{2} \ln y_{\text{TiO}_{2}}^{2} + y_{\text{ZrO}_{2}}^{2} \ln y_{\text{ZrO}_{2}}^{2} \right) + 0.5 \left(y_{\text{TiO}_{2}}^{3} \ln y_{\text{TiO}_{2}}^{3} + y_{\text{ZrO}_{2}}^{3} \ln y_{\text{ZrO}_{2}}^{3} \right) + 0.25 \left(y_{\text{CaO}}^{1} \ln y_{\text{CaO}}^{1} \right) \right] + G^{\text{ex},P}$$

$$(6)$$

where y_i^j represents the molar fraction of i in sub-lattice j, such as $y_{\text{TiO}_2}^2$ representing the molar fraction of TiO_2 in the second sub-lattice, $G_{\text{CaO:TiO}_2:\text{ZrO}_2}^0$ is the Gibbs free energy of end member, and $G^{\text{ex},P}$ is the excess Gibbs free energy of zirconolite and is defined as

$$\begin{split} G^{\text{ex},P} &= y_{\text{TiO}_2}^2 y_{\text{ZrO}_2}^2 (y_{\text{TiO}_2}^3 L_{\text{CaO:ZrO}_2,\text{TiO}_2;\text{TiO}_2} + \\ & y_{\text{ZrO}_2}^3 L_{\text{CaO:ZrO}_2,\text{TiO}_2;\text{ZrO}_2}) + y_{\text{TiO}_2}^3 y_{\text{ZrO}_2}^3 \; . \end{split}$$

$$(y_{\text{ZrO}_{2}}^{2}L_{\text{CaO:ZrO}_{2}:\text{ZrO}_{2},\text{TiO}_{2}}^{2} + y_{\text{TiO}_{2}}^{2}L_{\text{CaO:TiO}_{2}:\text{ZrO}_{2},\text{TiO}_{2}}^{2}) + y_{\text{CaO}}^{1}y_{\text{TiO}_{2}}^{2}y_{\text{ZrO}_{2}}^{2}y_{\text{TiO}_{2}}^{3}y_{\text{ZrO}_{2}}^{3}L_{\text{CaO:ZrO}_{2},\text{TiO}_{2}:\text{ZrO}_{2},\text{TiO}_{2}}^{2}$$
(7)

where $L_{\rm CaO:ZrO_2,TiO_2:ZrO_2}$ is the ternary interaction parameter.

4 Thermodynamic parameters

To obtain a set of consistent thermodynamic parameters of the ZrO₂-TiO₂-CaO system, the least square method was used to find the optimal values of interaction parameters. This method can obtain the best function matching of data by minimizing the sum of squares of errors using available information. Based on this principle, reliable equilibrium experiments and thermodynamic data were used as initial input data. However, some interaction parameters cannot be optimized successfully due to the lack of experimental information. Thus, the extrapolation principle of phase diagram was applied to the current work. For example, the binary interaction parameters of liquid phase can directly achieve ternary liquid by the extrapolation method. More details are shown in Table 1.

5 Results and discussion

5.1 Phase equilibrium

To assess the reliability of the present work, one should compare the experimental phase relationships and equilibria with calculations. The completely calculated diagram of ZrO₂-CaO-TiO₂ system at 1473 K is shown in Fig. 5, and its characteristics are captured: (1) zirconolite (CaZrTi₂O₇) and calzirtite (Ca₂Zr₅Ti₂O₁₆) are described as ternary phases with a homogeneity range between Zr and Ti; (2) zirconolite can directly achieve equilibrium with rutile, TiZrO₄, and O-CaTiO₃, leading to two ternary phase regions "rutile+CaZrTi₂O₇+TiZrO₄" and "rutile+ CaZrTi₂O₇+O-CaTiO₃"; (3) calzirtite extends and connects to the ZrO2-CaO system and the line of CaTiO₃-CaZrO₃, resulting in a ternary phase area " $Ca_2Zr_5Ti_2O_{16}+T_{ss}+O$ -CaTiO₃"; (4) the perovskite phases CaTiO₃ and CaZrO₃ form a series of continuous solid solutions; (5) CaZr₄O₉ expands to the line of CaTiO₃-CaZrO₃ because the Zr cations partly replace Ti cations. It should be noted that

 $\textbf{Table 1} \ Thermodynamic parameters of } ZrO_2\text{--}CaO\text{--}TiO_2 \ system$

Phase	Model	Ref.		
	$G_{\text{Liquid,TiO}_2}^0 = -915964.2 + 456.54037T - 77.76175T \ln T -$			
TiO ₂	$67156800T^{-2} + 1683920T^{-1} (298 - 3000 \text{ K})$			
	$G_{\text{TiO}_2}^{\text{Rutile}} = -976986.6 + 484.74037T - 77.76175T \ln T -$			
	$67156800T^{-2} + 1683920T^{-1} (298 - 3000 \text{ K})$			
	$G_{\text{Liquid,ZrO}_2}^0 = -1023332.5 + 387.7165T - 69.38751T \ln T -$			
	$3.7588 \times 10^{-3} T^2 + 683000 T^{-1} (298 - 3500 \text{ K})$			
	$G_{\text{ZrO}_2}^{\text{Cubic}} = -1110359.5 + 416.8908T - 69.38751T \ln T -$ $3.7588 \times 10^{-3} T^2 + 683000T^{-1} (298 - 3500 \text{ K})$			
7.0				
ZrO_2	$G_{ZrO_2}^{Tetragonal} = -1120695.5 + 420.8908T - 69.38751T \ln T -$	[7]		
	$3.7588 \times 10^{-3} T^2 + 683000 T^{-1} (298 - 3500 \text{ K})$			
	$G_{\text{ZrO}_2}^{\text{Monoclinic}} = -1126343.5 + 424.8908T - 69.38751T \ln T -$			
	$3.7588 \times 10^{-3} + 683000T^{-1} (298 - 3500 \text{ K})$			
	$(585630.85 + 300.6548T - 52.862T \ln T - 1.5545 \times 10^{-4}T^2 -$			
	$1.8919 \times 10^{-3} T^3 + 489415 T^{-1} (298 - 1830 \text{ K})$			
	$-793806 + 1510.99T - 212.7T \ln T + 5.49185 \times 10^{-2} T^2 -$			
	$G_{\text{Liquid,CaO}}^0 = \begin{cases} 3.79 \times 10^{-6} T^3 + 51730500 T^{-1} & (1830 - 2880 \text{ K}) \end{cases}$			
	$-4191941.7 + 15459T - 1961.2T \ln T + 0.45T^2 -$			
CaO	$2.102 \times 10^{-5} T^3 + 1.29186 \times 109 T^{-1} (2880 - 3172 \text{ K})$	[12]		
	$-663523.92 + 573.648794T - 84T \ln T $ (3172 – 6000 K)			
	$-653631.4 + 315.22123T - 51.8583T \ln T -$			
	$G_{\text{CaO}}^{\text{Periclase}} = \begin{cases} 0.0012193T^2 - 2.4 \times 10^{-11} T^3 + 468306 T^{-1} & (298 - 3172 \text{ K}) \\ 0.1436 & 2.2001821T + 227701T & 7.0045286 T^2 \end{cases}$			
	$G_{CaO} = 81436.3 - 2001.821T + 227.01T \ln T - 0.045386T^2 +$			
	$1.17 \times 10^{-6} T^3 - 3.48615 \times 10^8 T^{-1} (3172 - 6000 \text{ K})$			
$\mathrm{CaO}_{\mathrm{ss}}$	$G_{ ext{CaO}_{ ext{ss}}, ext{CaO}}^0 = G_{ ext{CaO}}^{ ext{Periclase}}$	[12]		
	$G_{a\text{-}Zr\text{TiO}_4, Zr\text{O}_2: \text{TiO}_2}^0 = G_{Zr\text{O}_2}^{\text{Monoclinic}} + G_{\text{TiO}_2}^{\text{Rutile}} + 8792.35 - 7.8904T$			
α-ZrTiO ₄	$G^0_{\beta-(Z_r,Ti)_2O_4,ZrO_2)} = G^{\text{Tetragonal}}_{ZrO_2} + 6200$	[8]		
	$G^0_{\beta - (\mathrm{Zr,Ti})_2 O_4, \mathrm{TiO}_2)} = G^{\mathrm{Rutile}}_{\mathrm{TiO}_2} + 6200$			
	$^{0}L_{\beta-(Zr,Ti)_{2}O_{4},ZrO_{2},TiO_{2}} = 7036.25 - 2.70274T$			
β -(Zr,Ti) ₂ O ₄	$^{1}L_{\beta-(Zr,Ti)_{2}O_{4},ZrO_{2},TiO_{2}} = 100$	[8]		
	$^{2}L_{\beta-(\mathrm{Zr,Ti})_{2}O_{4},\mathrm{ZrO}_{2},\mathrm{TiO}_{2}} = -900$			
	$G_{C_{ss},ZrO_2}^0 = G_{ZrO_2}^{\text{Cubic}}$	[7]		
	$G_{C_{\rm ss}, CaO}^0 = G_{CaO}^{\rm Liquid} - 17464 + 27.446T$	[/]		
	$G_{C_{ss},TiO_2}^0 = G_{TiO_2}^{Rutile} + 27900$	503		
	$^{0}L_{C_{ss},ZrO_{2},TiO_{2}} = 87850 - 20T$	[8]		
$C_{\rm ss}$	33 2 2			
$C_{\rm ss}$ (Cubic)	$^{1}L_{C_{ss},ZrO_{2},TiO_{2}} = -84900$	[7]		
	$^{1}L_{C_{ss},ZrO_{2},TiO_{2}} = -84900$ $^{2}L_{C_{ss},ZrO_{2},TiO_{2}} = 220394 - 73T$			
	$^{1}L_{C_{ss},ZrO_{2},TiO_{2}} = -84900$			

(Continued)

Phase	Model	Ref.	
	$G_{T_{\rm ss}, {\rm ZrO}_2}^0 = G_{{\rm ZrO}_2}^{\rm Tetragonal}$	[7]	
	$G_{T_{ss},\text{CaO}}^{0} = G_{\text{CaO}}^{\text{Liquid}} + 27724 + 27.446T$ $G_{T_{ss},\text{TiO}_{2}}^{0} = G_{\text{TiO}_{2}}^{\text{Rutile}} + 35000$		
$T_{ m ss}$	$^{0}L_{T_{ss},ZrO_{2},CaO} = -41982.6 - 17.5437T$	[8]	
(Tetragonal)	$^{0}L_{T_{\text{ss}},Zro_{2},CaO} = -15061 - 5.85724T$		
	$^{1}L_{T_{ss},ZrO_{2},TriO_{2}} = 2441.81 + 9.05699T$	[7]	
	$^{2}L_{T_{ss},ZrO_{2},TiO_{2}} = 2101$	This work	
	$^{0}L_{T_{ss},ZrO_{2},TiO_{2},CaO} = 2854.5$	THIS WOLK	
	$G^0_{M_{_{\mathrm{SS}}},\mathrm{ZrO}_2} = G^{\mathrm{Monoclinic}}_{\mathrm{ZrO}_2}$	[8]	
	$G_{M_{ m ss},{ m CaO}}^0 = G_{{ m CaO}}^{ m Liquid} + 2500$	[0]	
$M_{ m ss}$	$G_{M_{\rm ss}, \text{TiO}_2}^0 = G_{\text{TiO}_2}^{\text{Rutile}} - 5858 + 13.388T$	[7]	
(Monoclinic)	$^{0}L_{M_{ss},ZrO_{2},TiO_{2}} = 32885.2 - 6.38468T$	[/]	
	$^{0}L_{M_{\rm ss},\rm ZrO_{2},\rm CaO} = 58647 - 13T$	This work	
	$^{0}L_{T_{ss},ZrO_{2},TiO_{2},CaO} = 2578.9$	Tills Work	
	$G^0_{ m Liquid,ZrO_2}, G^0_{ m Liquid,TiO_2}, G^0_{ m Liquid,CaO}$	This work	
	$^{0}L_{\text{Liquid,TiO}_{2},\text{CaO}} = -186214 + 2.1138T$	THIS WOLK	
	$^{1}L_{\text{Liquid,TiO}_{2},\text{CaO}} = -22936.8$	[7]	
Liquid	$^{0}L_{\text{Liquid,ZrO}_{2},\text{CaO}} = -169081 + 27.694T$	F. J	
1	$^{0}L_{\text{Liquid,ZrO}_{2},\text{TiO}_{2}} = -87957 + 27.7469T$	[8]	
	$^{1}L_{\text{Liquid,ZrO}_{2},\text{TiO}_{2}} = 26104.6 - 18T$	This work	
	$^{2}L_{\text{Liquid,ZrO}_{2},\text{TiO}_{2}} = 45082.2 - 20T$		
	$^{0}L_{\text{Liquid,ZrO}_{2},\text{TiO}_{2}:\text{CaO}} = -2000$		
	$G^0_{ m Rutile, TiO_2} = G^{ m Rutile}_{ m TiO_2}$		
Rutile	$G_{\text{Rutile,ZrO}_2}^0 = G_{\text{ZrO}_2}^{\text{Tetragonal}} + 36000$	[8]	
Ruthe	$^{0}L_{\text{Rutile,ZrO}_{2},\text{TiO}_{2}} = 35374.2 - 29.662T$		
	$^{1}L_{\text{Rutile,ZrO}_{2},\text{TiO}_{2}} = -41519.8 + 30.38T$		
$ZrTi_2O_6$	$G_{\rm ZrTi_2O_6,ZrO_2:TiO_2}^0 = G_{\rm ZrO_2}^{\rm Monoclinic} + 2G_{\rm TiO_2}^{\rm Rutile} - 11501 + 6.6866T$	[8]	
T-CaTiO₃	$G_{\text{T-CaTiO}_3,\text{TiO}_2:\text{CaO}}^0 = 0.5G_{\text{CaO}}^{\text{Periclase}} + 0.5G_{\text{TiO}_2}^{\text{Rutile}} - 40163.5 - 3.5987T$	[12]	
CCZT (C-Ca(Zr,Ti)O ₃)	$G_{\text{CCZT,TiO}_2:\text{CaO}}^0 = 0.5G_{\text{CaO}}^{\text{Periclase}} + 0.5G_{\text{TiO}_2}^{\text{Rutile}} - 40081.75 - 3.6487T$	This work	
	$G_{\rm CCZT,ZrO_2:CaO}^0 = 0.5G_{\rm CaO}^{\rm Periclase} + 0.5G_{\rm ZrO_2}^{\rm Monoclinic} - 11428.7 - 7.2601T$	[7]	
	$G_{\text{CCZT},\text{ZrO}_2,\text{TiO}_2;\text{CaO}}^0 = 20000$	This work	
	$G_{\rm Ph1,ZrO_2:CaO}^0 = 0.2G_{\rm CaO}^{\rm Periclase} + 0.8G_{\rm ZrO_2}^{\rm Monoclinic} + 3120.15 - 9.3823T$		
CaZr ₄ O ₉	$G^0_{ m Ph1,TiO_2:CaO} = 0.2G^{ m Periclase}_{ m CaO} + 0.8G^{ m Rutile}_{ m TiO_2}$	This work	
	$G_{\text{Ph1,ZrO}_2,\text{TiO}_2:\text{CaO}}^0 = -126937.625 + 67.5T$		
Ca ₆ Zr ₁₉ O ₄₄	$G_{\text{Ph}2,\text{ZrO}_2:\text{CaO}}^0 = 0.24 G_{\text{CaO}}^{\text{Periclase}} + 0.76 G_{\text{ZrO}_2}^{\text{Monoclinic}} - 3601.25 - 5.8752T$	[8]	

(Continued)

Phase	Model	Ref.
$Ca_3Ti_2O_7$	$G_{\text{Ca}_{3}\text{Ti}_{2}\text{O}_{7},\text{TiO}_{2}:\text{CaO}}^{0} = 0.6G_{\text{CaO}}^{\text{Periclase}} + 0.4G_{\text{TiO}_{2}}^{\text{Rutile}} - 32863.4 - 3.3476T$	[12]
$Ca_4Ti_3O_{10}$	$G_{\text{Ca}_{4}\text{Ti}_{3}\text{O}_{10},\text{TiO}_{2}:\text{CaO}}^{0} = 0.57 G_{\text{CaO}}^{\text{Periclase}} + 0.43 G_{\text{TiO}_{2}}^{\text{Rutile}} - 35124.714 - 3.465 T$	[12]
OCZT (O-Ca(Zr,Ti)O ₃)	$G_{\text{OCZT,TiO}_2:\text{CaO}}^0 = 0.5G_{\text{CaO}}^{\text{Periclase}} + 0.5G_{\text{TiO}_2}^{\text{Rutile}} - 40847.25 - 3.1487T$ $G_{\text{OCZT,ZrO}_2:\text{CaO}}^0 = 0.5G_{\text{CaO}}^{\text{Periclase}} + 0.5G_{\text{ZrO}_2}^{\text{Monoclinic}} - 15975 - 5.2601T$	This work
CZT ₂ (Zirconolite)	$\begin{split} G^0_{\text{CZT}_2,\text{TiO}_2:\text{CaO}:\text{ZrO}_2} &= G^{\text{Monoclinic}}_{\text{ZrO}_2} + G^{\text{Periclase}}_{\text{CaO}} + 2G^{\text{Rutile}}_{\text{TiO}_2} - 162010.25 + 22T \\ G^0_{\text{CZT}_2,\text{ZrO}_2:\text{TiO}_2:\text{CaO}} &= 3G^{\text{Monoclinic}}_{\text{ZrO}_2} + G^{\text{Periclase}}_{\text{CaO}} + 10000 \\ G^0_{\text{CZT}_2,\text{ZrO}_2:\text{CaO}:\text{TiO}_2} &= 2G^{\text{Monoclinic}}_{\text{ZrO}_2} + G^{\text{Periclase}}_{\text{CaO}} + G^{\text{Rutile}}_{\text{TiO}_2} \\ G^0_{\text{CZT}_2,\text{TiO}_2:\text{CaO}:\text{TiO}_2} &= G^{\text{Periclase}}_{\text{CaO}} + 3G^{\text{Rutile}}_{\text{TiO}_2} - 50000 \end{split}$	This work
$C_2Z_5T_2$ (Calzirtite)	$\begin{split} G^{0}_{\text{C}_2\text{Z}_5\text{T}_2,\text{TiO}_2:\text{CaO}:\text{ZrO}_2} &= 5G_{\text{ZrO}_2}^{\text{Monoclinic}} + 2G_{\text{CaO}}^{\text{Periclase}} + 2G_{\text{TiO}_2}^{\text{Rutile}} + T - 201473 \\ G^{0}_{\text{C}_2\text{Z}_5\text{T}_2,\text{ZrO}_2:\text{TiO}_2:\text{CaO}} &= 7G_{\text{ZrO}_2}^{\text{Monoclinic}} + 2G_{\text{CaO}}^{\text{Periclase}} \\ G^{0}_{\text{C}_2\text{Z}_5\text{T}_2,\text{ZrO}_2:\text{CaO}:\text{TiO}_2} &= 2G_{\text{ZrO}_2}^{\text{Monoclinic}} + 2G_{\text{CaO}}^{\text{Periclase}} + 5G_{\text{TiO}_2}^{\text{Rutile}} - 62000 - 13.5T \\ G^{0}_{\text{C}_2\text{Z}_5\text{T}_2,\text{TiO}_2:\text{CaO}:\text{TiO}_2} &= 2G_{\text{CaO}}^{\text{Periclase}} + 7G_{\text{TiO}_2}^{\text{Rutile}} - 40007.64 \\ G^{0}_{\text{C}_2\text{Z}_5\text{T}_2,\text{ZrO}_2,\text{TiO}_2:\text{CaO}:\text{TiO}_2,\text{ZrO}_2} &= 10007.56 \end{split}$	This work

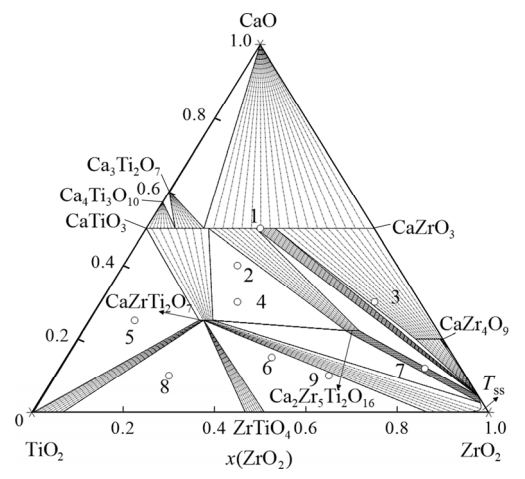


Fig. 5 Isothermal sections of ZrO₂–CaO–TiO₂ system at 1473 K compared with experimental data [1]

the calculated homogeneity ranges of ZrO_2 in zirconolite and calzirtite are respectively identified as 23%-27% (molar fraction) and 57%-61% (molar fraction), and are similar to 21%-29% (molar fraction) and 54%-61% (molar fraction) in the experiments of SWENSON et al [1].

With the temperature increasing to 1673 K, the phase relationships of ZrO₂–CaO–TiO₂ system undergo a significant variation. As shown in Fig. 6, the Ca₂Zr₅Ti₂O₁₆ and CaZr₄O₉ phases disappear at 1673 K, meanwhile, the CaZrTi₂O₇ connects to the ZrO₂-rich side, and leads to a new ternary phase area (CaZrTi₂O₇ +*T*ss + CaTiO₃). It should be noted that part of the experimental data from PREDA et al [16] are considered in the present work.

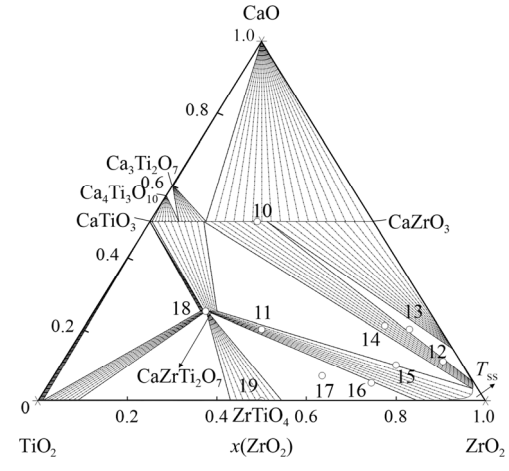


Fig. 6 Isothermal sections of ZrO₂–CaO–TiO₂ system at 1673 K compared with experimental data [16]

In this work, the calculated diagram of ZrO₂–CaO–TiO₂ system at 1473 K is in agreement with the experimental results of SWENSON et al [1], except for the phase relationships between $C_{\rm ss}$ and calzirtite. In their work, the phase relationships are completely extrapolated from experimental results. However, the experiments contain thermodynamic nonequilibrium problems, which may be the reason for the differences. The calculated diagram of the ZrO₂–CaO–TiO₂ system at 1673 K is consistent with the measurements of phase relationships [16], but the calculated phase boundaries at the ZrO₂-rich corner deviate slightly from the experimental results, which are within the permissible range of experimental errors.

As shown in Table 2 and Table 3, there exist differences between the experiments and the calculation at the ZrO₂-rich corner, where the $M_{\rm ss}$ phases are replaced by the $T_{\rm ss}$ phases in this work. The differences can be attributed to two reasons. On the one hand, the equilibrium phase boundaries between C_{ss} , M_{ss} , and T_{ss} can hardly be established at the ZrO₂-rich corner especially below 1473 K, for example, at 1373 K, the metastable transition needs more than 70 years to reach equilibrium due to the sluggish kinetics of cations from the research of YASHIMA et al [24]; on the other hand, as temperature rises above 1473 K, the energy of $T_{\rm ss}$ phase is smaller than that of the M_{ss} phase; thus, the metastable phase at the ZrO₂-rich corner at 1473 and 1673 K is described as $T_{\rm ss}$ in the present work,

which is consistent with SWENSON et al [1] and PREDA et al [16]. Apart from that, there are 19 experimental points listed in Table 2 and Table 3, and most of the results keep a good agreement with our calculation except for 5 experimental points. More details are described below.

(1) Samples 2 and 6: The difference may be caused by experimental error, because it is difficult to achieve an ideal equilibrium in phase diagram experiments under the influence of thermodynamics, dynamics, and experimental conditions, especially for zirconia-based systems. Besides, SWENSON et al [1] pointed out that some samples, such as Sample 6, are not at thermodynamic equilibrium at 1473 K. Thus, our optimized results may be more credible.

Table 2 Comparison of results between experimental data [1] and calculated results at 1473 K

Sample No.	Sample No. Molar fraction/%		on/%	Phase		
in Fig. 5	CaO	TiO ₂	ZrO_2	Experimental	Calculated	Agreement
1	0.50	0.25	0.25	CaZrO ₃ +CaTiO ₃	Ca(Zr, Ti)O ₃	Yes
2	0.40	0.35	0.25	$CaTiO_3+C_{ss}+Ca_2Zr_5Ti_2O_{16}$	$CaTiO_3 + CaZrTi_2O_7 + Ca_2Zr_5Ti_2O_{16}$	No
3	0.30	0.10	0.60	CaZrO ₃ +CaZr ₄ O ₉	CaZrO ₃ +CaZr ₄ O ₉	Yes
4	0.30	0.40	0.30	$CaTiO_3 + CaZrTi_2O_7 + Ca_2Zr_5Ti_2O_{16}$	$CaTiO_3 + CaZrTi_2O_7 + Ca_2Zr_5Ti_2O_{16}$	Yes
5	0.25	0.65	0.10	CaTiO ₃ +CaZrTi ₂ O ₇ +TiO ₂	CaTiO ₃ +CaZrTi ₂ O ₇ +TiO ₂	Yes
6	0.15	0.40	0.45	CaTiO ₃ +CaZrTi ₂ O ₇ +TiO ₂	CaTiO ₃ +CaZrTi ₂ O ₇ + TiZrO ₄	No
7	0.12	0.8	0.80	$M_{\rm ss}$ +CaZrTi ₂ O ₇	$T_{\rm ss}$ +CaZrTi ₂ O ₇	Yes
8	0.10	0.65	0.25	$TiZrO_4 + CaZrTi_2O_7 + TiO_2$	$TiZrO_4 + CaZrTi_2O_7 + TiO_2$	Yes
9	0.10	0.30	0.60	$M_{\rm ss}$ +CaZrTi ₂ O ₇	$T_{\rm ss}$ +CaZrTi ₂ O ₇	Yes

Table 3 Comparison of results between experimental data [16] and calculated results at 1673 K

Sample No.	Molar fraction/%			Phase		A
in Fig. 6	CaO	TiO ₂	ZrO_2	Experimental	Calculated	- Agreement
10	0.24	0.26	0.5	CaZrO ₃ +CaTiO ₃	Ca(Zr, Ti)O ₃	Yes
11	0.4	0.4	0.2	$M_{\rm ss}$ +CaZrTi ₂ O ₇	$T_{\rm ss}$ +CaZrTi ₂ O ₇	Yes
12	0.85	0.04	0.11	$M_{ m ss}$ +Css	$T_{\rm ss}$ +CaTiO ₃	No
13	0.73	0.07	0.2	$C_{ m ss}$	T_{ss} +Css+CaTiO ₃	No
14	0.67	0.12	0.21	$M_{\rm ss}+C_{\rm ss}+{\rm CaTiO_3}$	$T_{\rm ss}$ +CaTiO ₃	No
15	0.75	0.15	0.1	$M_{\rm ss}$ +CaZrTi ₂ O ₇	$T_{\rm ss}$ +CaZrTi ₂ O ₇	Yes
16	0.72	0.23	0.05	$M_{\rm ss}$ +CaZrTi ₂ O ₇ +TiZrO ₄	T_{ss} +CaZrTi ₂ O ₇ +TiZrO ₄	Yes
17	0.6	0.33	0.07	$M_{\rm ss}$ +CaZrTi ₂ O ₇ +TiZrO ₄	T _{ss} +CaZrTi ₂ O ₇ + TiZrO ₄	Yes
18	0	0.5	0.5	$TiZrO_4$	$TiZrO_4$	Yes
19	0.25	0.5	0.25	CaZrTi ₂ O ₇	CaZrTi ₂ O ₇	Yes

(2) Samples 12–14: In the experiments of PREDA et al [16], the samples were thermally treated at 1673 K for 2 h. It seems that their diagrams are nonequilibrium during a very short period of holding time, especially for the ZrO₂-rich corner. It was proposed by YASHIMA et al [24] that most of the experimental data at the ZrO₂-rich corner were not accurate. Thus, the experiment points for Samples 12–14 as shown in Table 3 may be unreliable.

Based on three binary systems (TiO₂–CaO, ZrO₂–CaO, and ZrO₂–TiO₂), and experimental data from SWENSON et al [1] and PREDA et al [16], a set of self-consistent thermodynamic parameters are obtained, which can well describe the isothermal sections at 1473 and 1673 K, and forecast the isothermal sections at higher temperatures [25–27]. As shown in Fig. 7, the calculated results are in agreement with the experimental ones at 1723 K. As the temperature rises to 1773 K, part of the rutile

(TiO₂) has transformed into liquid, which is consistent with the results of TiO2-CaO binary system. Also, our present thermodynamic database can be used to design and prepare refractory material for melting alloy [28] by machine [29–31] and high-throughput thermodynamic calculations [32–34]. As shown in Fig. 8, the liquidus temperatures contain 900 materials with different compositions by high-throughput thermodynamic calculations, which is helpful for understanding the changing law of melting point of materials. It should be noted that the solid solubilities of rutile, C_{ss} and T_{ss} are neglected due to a lack of experimental information, and the predicted decomposition temperature Ca₂Zr₅Ti₂O₁₆ is 1656 K.

5.2 Thermodynamic properties of CaZrTi₂O₇

Until now, only thermodynamic information of CaZrTi₂O₇ has been reported by several researchers.

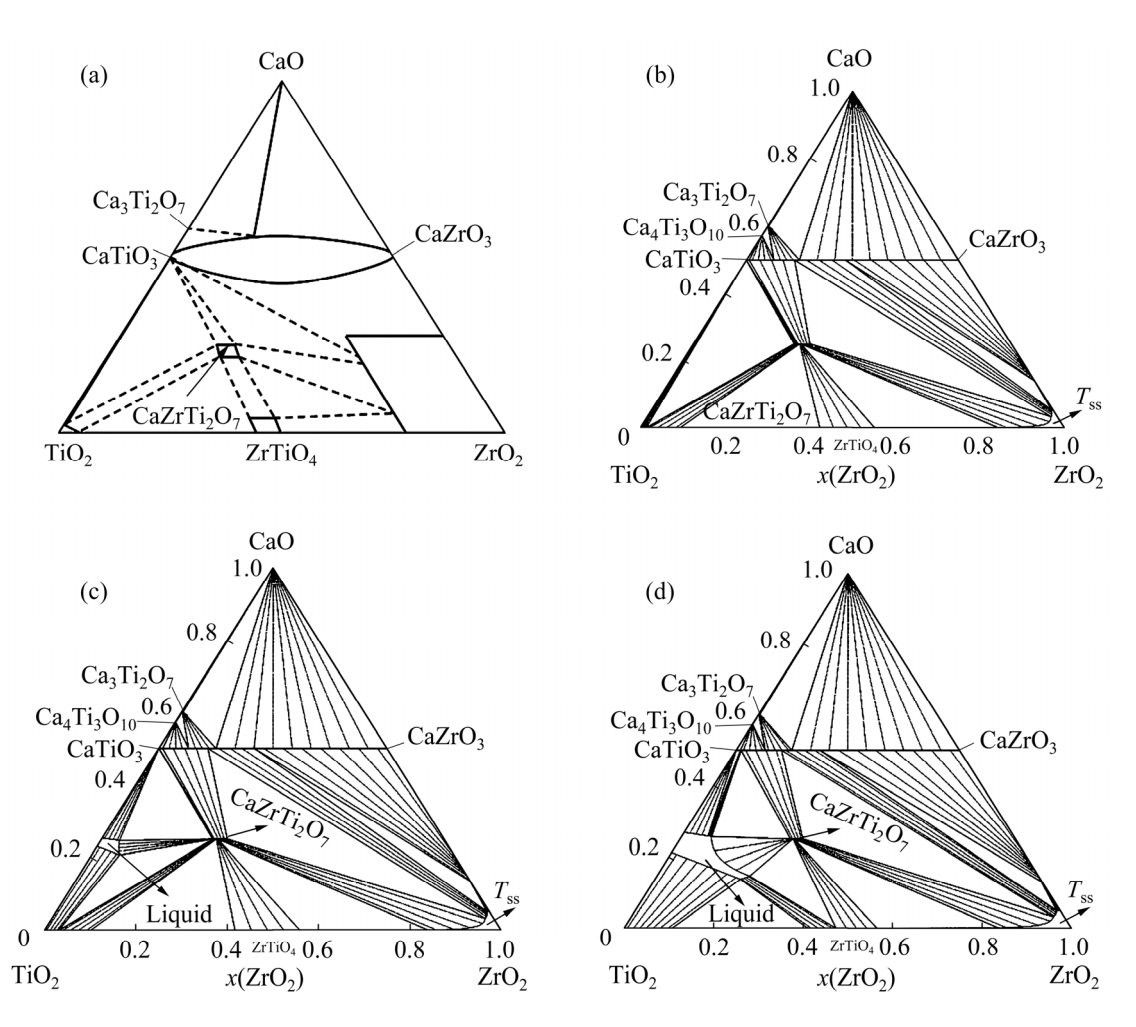


Fig. 7 Calculated phase relationships of ZrO₂–CaO–TiO₂ system compared with experimental results in Ref. [14]: (a) Estimated trends of solid–solution development in temperature range of 1723–1823 K; (b–d) Isothermal sections at 1723 K (b), 1773 K (c) and 1823 K (d) in this work

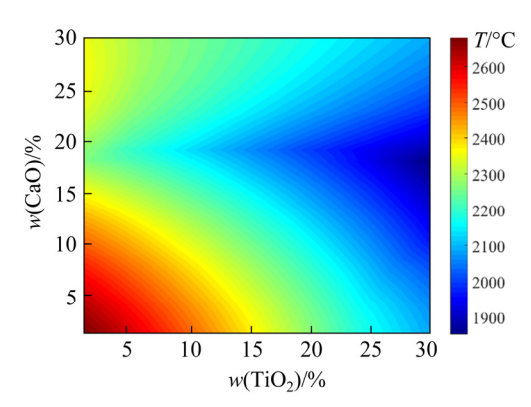


Fig. 8 Colormap of liquidus temperatures by highthroughput thermodynamic calculations

The specific heat capacity, the standard molar enthalpy of formation, and entropy of CaZrTi₂O₇ were reported completely by PÖML et al [35], PUTNAM et al [36], and WOODFIELD et al [37]. Their thermodynamic data were used in the present optimization. In the work of PÖML et al [35], a series of enthalpy increment experiments were carried out by using drop calorimetry. The hightemperature specific heat capacity of CaZrTi₂O₇ was confirmed by combining the enthalpy increment measurements and low-temperature specific heat capacity data. WOODFIELD et al [37] measured the specific heat capacity using an adiabatic calorimeter, following which a six-term fitting equation based on the Debye and Einstein functions has been shown to represent the specific heat capacity over the entire range of temperatures. As shown in Fig. 9, our present work was different from WOODFIELD et al [37], but was in good agreement with the results of in Ref. [35] within 5% errors.

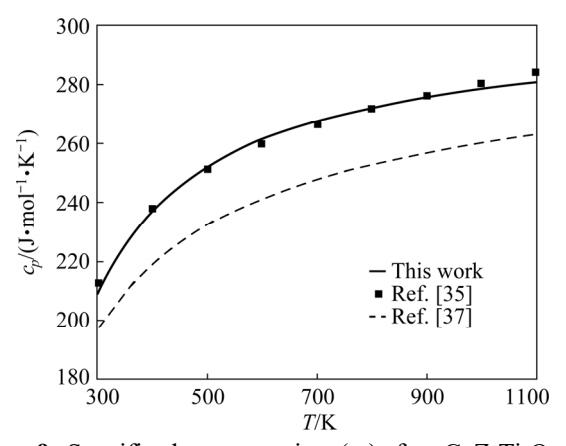


Fig. 9 Specific heat capacity (c_p) for CaZrTi₂O₇ at 298.15–1100 K compared with experimental data from Refs. [35,37]

Utilizing the high-temperature oxide-melt solution calorimetry, PUTNAM et al [36] determined the standard molar heat enthalpy of formation at 298.15 K for CaZrTi₂O₇. The value is shown in Table 4. Also, a series of entropy data for CaZrTi₂O₇ were confirmed by PÖML et al [35], PUTNAM et al [36], and WOODFIELD et al [37] applying the same methods. As shown in Fig. 10, the calculated results can well simulate the experimental results, and the errors are less than 5%.

Table 4 Standard heat enthalpy from all elements and specific heat capacity of CaZrTi₂O₇ compared with experimental data in Refs. [35,36]

$\Delta H_{ m f, 298.15 \ K}/\ m (kJ \cdot mol^{-1})$	$c_{p298.15 \text{ K}}/$ $(\text{J} \cdot \text{mol}^{-1} \cdot \text{K}^{-1})$	Source
-	211.9	Ref. [35]
-3713.7 ± 4.5	_	Ref. [36]
-3784.2	208.5	This work

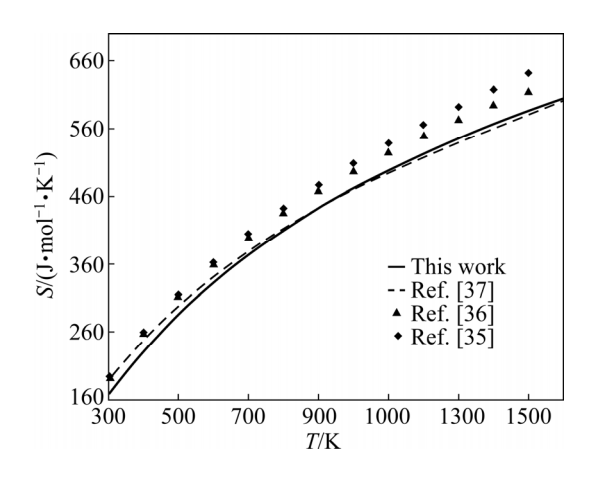


Fig. 10 Entropy (S) of $CaZrTi_2O_7$ at 300–1600 K compared with experimental data from Refs. [35–37]

5.3 Vertical section of CaTiO₃-CaZrO₃

According to Refs. [1,14], the liquid and solid phases based on the CaTiO₃–CaZrO₃ system are characterized by mutual solubility. To well describe the vertical section, the liquid and solid phases are treated as ternary ideal solutions and are modeled as substitutional solution models. As shown in Fig. 11, there are a series of continuous solid solutions between the two perovskite phases, which are consistent with the results in Refs. [1,14]. It is noted that the solid–liquid boundary is extrapolated in this work due to a lack of phase equilibrium information.

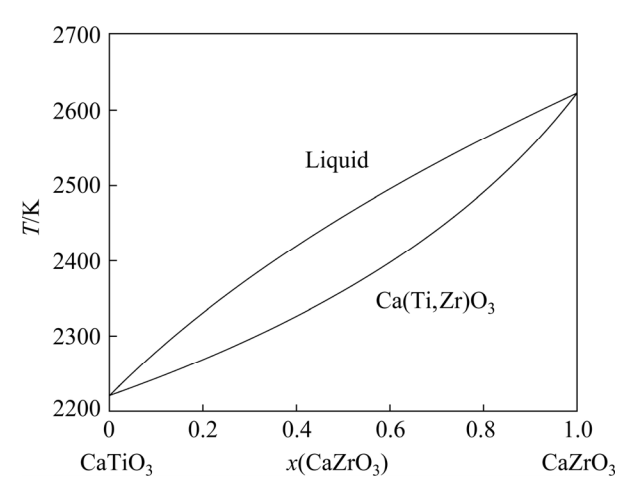


Fig. 11 Calculated vertical section of CaTiO₃-CaZrO₃ system

6 Conclusions

- (1) The thermodynamic functions of the ZrO₂–CaO–TiO₂ system are evaluated, and the results show a satisfactory agreement with the experimental isothermal sections reported recently at 1473 and 1673 K. The specific heat capacity and other thermodynamic properties of zirconolite are successfully calculated, which are consistent with experiments, and the errors are less than 5%.
- (2) The thermodynamic models for zirconolite and calzirtite are identified as Ca(Zr,Ti)(Ti,Zr)₂O₇ and Ca₂(Zr,Ti)₅(Ti,Zr)₂O₁₆, respectively. The homogeneity ranges of ZrO₂ in zirconolite and calzirtite are 23%–27% (molar fraction) and 57%–61% (molar fraction) at 1473 K, which are similar to experimental values (21%–29% (molar fraction) and 54%–61% (molar fraction)).
- (3) Compared to 19 experimental points in the ZrO₂–CaO–TiO₂ system, 5 experimental points are not consistent with our calculation results. The reasons are attributed to experimental errors and the sluggish kinetics of cations for ZrO₂-based materials.

Acknowledgments

The authors are grateful for the financial supports from the Open Project of State Key Laboratory of Advanced Special Steel and Shanghai Key Laboratory of Advanced Ferrometallurgy, China (No. SKLASS2019-11), and the National Natural Science Foundation of China (No. 52104305).

References

- [1] SWENSON D, NIEH T, FOURNELLE J. The CaO-TiO₂-ZrO₂ system at 1200 °C and the solubilities of Hf and Gd in zirconolite [J]. Materials Research Society, 1995, 412: 337-344.
- [2] CHEN Rui, LIU Rui-jing, CHEN Cun, HU Hai-feng, CHEN Li-hui, GAO Jing, LI Guo-hua. Mesoporous titania microsphere self-assembled by nano-slices with preferential crystallographic orientation and its formation mechanism [J]. Transactions of Nonferrous Metals Society of China, 2020, 30: 1602–1610.
- [3] POLISETTI S, DESHPANDE P A, MADRAS G. Photocatalytic activity of combustion synthesized ZrO₂ and ZrO₂-TiO₂ mixed oxides [J]. Industrial & Engineering Chemistry Research, 2011, 50: 12915–12924.
- [4] KANG Ju-yun, CHEN Guang-yao, LAN Bao-bao, LI Bao-tong, LU Xiong-gang, LI Chong-he. Stability of Y-doped BaZrO₃ and its erosion resistance of titanium melts [J]. Transactions of Nonferrous Metals Society of China, 2019, 29: 749-755.
- [5] ZHOU Ru-hai, CHEN Guang-yao, LI Bao-tong, ALI W, LU Xiong-gang, LI Chong-he. Microstructure evolution of Y₂O₃ doped BaZrO₃ and its interface reaction with titanium melt [J]. Transactions of Nonferrous Metals Society of China, 2017, 27: 2276–2282.
- [6] CHEN Ming, HALLSTEDT B, GAUCKLER L J. Thermodynamic modeling of the ZrO₂–YO_{1.5} system [J]. Solid State Ionics, 2004, 170: 255–274.
- [7] WANG Kun, LI Chong-he, GAO Yu-lai, LU Xiong-gang, DING Wei-zhong. Thermodynamic reassessment of ZrO₂— CaO system [J]. Journal of the American Ceramic Society, 2009, 92: 1098–1104.
- [8] HE Shi-yu, LIU Xiao-mei, FENG Qi-sheng, ZOU Xing-li, WU Zhu, LI Chong-he, LU Xiong-gang. Thermodynamic assessments of ZrO₂-YO_{1.5}-TiO₂ system [J]. Ceramics International, 2021, 41: 3525–3534.
- [9] UMEZU S. Investigation on the iron blast furnace slag containing titanium [J]. Journal of Mining and Metallurgical Institute of Japan, 1930, 46: 867–877.
- [10] DEVRIES R C, ROY R, OSBORN E F. Phase equilibria in the system CaO–TiO₂ [J]. The Journal of Physical Chemistry, 1955, 38: 1069–1073.
- [11] ROTH R S. Revision of the phase equilibrium diagram of the binary system calcia–titania, showing the compound $Ca_4Ti_3O_{10}$ [J]. Journal of Research of the National Bureau of Standards, 1958, 61: 437–440.
- [12] GONG Wei-ping, WU Li-li, NAVROTSKY A. Combined experimental and computational investigation of thermodynamics and phase equilibria in the CaO-TiO₂ system [J]. Journal of the American Ceramic Society, 2018, 101: 1361–1370.
- [13] IIKKA I, ZHANG Rui, XIA Long-fan, NIKO H, PEKKA A. Thermodynamic assessment of ZnO-SiO₂ system [J]. Transactions of Nonferrous Metals Society of China, 2018, 28: 1869–1877
- [14] COUGHANOUR W, ROTH R. Solid-state reactions and dielectric properties systems magnesia-zirconia-titania and zirconia-titania [J]. Journal of Research of the National Bureau of Standards, 1955, 54: 191-199.
- [15] FIGUEIREDO M O, SANTOS D A C, CORTINA C P, BASTO M J. The pyrochlore line in the system

- CaO-ZrO₂-TiO₂: Implications on synroc phase assemblages [J]. Materials Research Society, 1991, 257: 251-256.
- [16] PREDA M, REHNER H, NICOLESCU C. The stabilization of zirconium dioxide in the ternary system CaO-TiO₂-ZrO₂
 [J]. Journal of the European Ceramic Society, 1997, 17: 891-896.
- [17] ROSSELL H. Calzirtite—A fluorite-related superstructure [J]. Acta Crystallographica (Section B): Structural Crystallography and Crystal Chemistry, 1982, 38: 593–595.
- [18] PYATENKO Y A, PUDOVKINA Z V. The crystal structure of calcirtite: A new derivative structure of CaF₂-CeO₂ type [J]. Kristallografiya, 1961, 6: 196–199.
- [19] ASADIKIYA M, FOROUGHI P, ZHONG Yu. Re-evaluation of the thermodynamic equilibria on the zirconia-rich side of the ZrO₂-YO_{1.5} system [J]. CALPHAD, 2018, 61: 264–274.
- [20] KAUFMAN L. Calculation of multicomponent ceramic phase diagrams [J]. Physica B+C, 1988, 150: 99–114.
- [21] KIRSCHEN M, DECAPITANI C. Experimental determination and computation of the liquid miscibility gap in the system CaO-MgO-SiO₂-TiO₂ [J]. Journal of Phase Equilibria, 1999, 20: 593-611.
- [22] DANĚK V, NERÁD I. Phase diagram and structure of melts of the system CaO-TiO₂-SiO₂ [J]. Chemical Papers, 2002, 56: 241-246.
- [23] VANCE E, CASSIDY D, BALL C J, THOROGOOD G J. High-temperature study of CaZrTi₂O₇ [J]. Journal of Nuclear Materials, 1992, 190: 295–297.
- [24] YASHIMA M, KAKIHANA M, YOSHIMURA M. Metastable-stable phase diagrams in the zirconia-containing systems utilized in solid-oxide fuel cell application [J]. Solid State Ionics, 1996, 86: 1131–1149.
- [25] LIN Chong-mao, WANG Shu-sen, CHEN Guang-yao, WANG Kun, CHENG Zhi-wei, LU Xiong-gang, LI Chong-he. Thermodynamic evaluation of the BaO–ZrO₂–YO_{1.5} system [J]. Ceramics International, 2016, 42: 13738–13747.
- [26] LI Zhu, WANG Jing, LI Bao-tong, WANG Shu-sen, ALI W, WANG Shi-hua, WANG Xue-guang, LU Xiong-gang, LI Chong-he, WANG Kun. Thermodynamic evaluation of the BaO-CaO- YO' system [J]. Journal of the European Ceramic Society, 2017, 38: 323-332.
- [27] LIU Xiao-mei, LI Zhu, WANG Jing, ZHANG Rui-lin, ALI W, WANG Shi-hua, LU Xiong-gang, LI Chong-he. Phase equilibria and thermodynamic evaluation of BaO-TiO₂-YO_{1.5} system [J]. Journal of the European Ceramic Society, 2018, 38:

- 5430-5441.
- [28] ZHAO Jun-chao, LIU Zheng, LI Ze-wen, SUN Meng-tong. Effect of electromagnetic stirring parameters on melt flow and microstructure of semi-solid aluminum alloy melts in oval crucible [J]. Transactions of Nonferrous Metals Society of China, 2020, 30: 1523–1534.
- [29] JHA R, CHAKRABORTI N, DIERCKS D R. Combined machine learning and CALPHAD approach for discovering processing-structure relationships in soft magnetic alloys [J]. Computational Materials Science, 2018, 150: 202–211.
- [30] ZENG Yin-zhi, MAN Meng-ren, BAI Ke-wu, ZHANG Yong-wei. Revealing high-fidelity phase selection rules for high entropy alloys: A combined CALPHAD and machine learning study [J]. Materials & Design, 2021, 202(8): 109532.
- [31] PAN Yu-hang, ZHOU Ping, YAN Ying, AGRAWAL A, WANG Yong-hao, GUO Dong-ming, GOEL S. New insights into the methods for predicting ground surface roughness in the age of digitalisation [J]. Precision Engineering, 2021, 67: 393–418
- [32] CURTAROLO S, HART G L W, NARDELLI M B, MINGO N, SANVITO S, LEVY, O. The high-throughput highway to computational materials design [J]. Nature Materials, 2013, 12: 191–201.
- [33] SORKIN V, TAN T L, YU Z G, ZHANG Y W. Highthroughput calculations based on the small set of ordered structures method for non-equimolar high entropy alloys [J]. Computational Materials Science, 2021, 188: 110213.
- [34] ZHANG Cong, JIANG Xue, ZHANG Rui-jie, WANG Xin, YIN Hai-qing, QU Xuan-hui, LIU Zi-kui. High-throughput thermodynamic calculations of phase equilibria in solidified 6016 Al-alloys [J]. Computational Materials Science, 2019, 167: 19–24.
- [35] PÖML P, GEISLER T, KONINGS R. High-temperature heat capacity of zirconolite (CaZrTi₂O₇) [J]. The Journal of Chemical Thermodynamics, 2006, 38: 1013–1018.
- [36] PUTNAM R L, NAVROTSKY A, WOODFIELD B F, GOATES B J, SHAPIRO J L. Thermodynamics of formation for zirconolite (CaZrTi₂O₇) from *T*=298.15 K to *T*=1500 K [J]. The Journal of Chemical Thermodynamics, 1999, 31: 229–243.
- [37] WOODFIELD B F, BOERIO-GOATES J, SHAPIRO J L, PUTNAM R L, NAVROTSKY A. Molar heat capacity and thermodynamic functions of zirconolite CaZrTi₂O₇ [J]. Journal of Chemical Thermodynamics, 1999, 31: 245–253.

ZrO2-CaO-TiO2体系的热力学模拟

何世宇^{1,2}, 冯齐胜^{1,2}, 段保华^{1,2}, 陈光耀^{1,2}, 吴 铸³, 李重河^{1,2}, 鲁雄刚^{1,2,4}

- 1. 上海大学 材料科学与工程学院 省部共建高品质特殊钢冶金与制备国家重点实验室 上海市钢铁冶金新技术开发应用重点实验室,上海 200444;
- 2. 上海特种铸造工程技术研究中心,上海 201605; 3. 中国科学院 上海微系统与信息技术研究所,上海 201800; 4. 上海电机学院 材料学院,上海 201306
 - 摘 要: ZrO_2 -CaO-TiO₂ 体系相图对光催化材料和耐火材料的发展至关重要。采用 CALPHAD 方法研究 ZrO_2 -CaO-TiO₂ 体系。亚正规溶体模型用于描述液相和固溶相,亚点阵模型用于描述三元化合物。然后,结合文献实验结果,利用最小二乘法得到热力学参数。应用本研究优化的热力学参数,计算 1473 和 1673 K 下 ZrO_2 -CaO-TiO₂ 的等温截面,实验和计算的相关系吻合很好,部分不匹配的实验点误差可归结于实验误差和氧化锆基材料的动力学缓慢特性。为了进一步证实该数据库的有效性,利用该数据库模拟 ZrO_2 -CaO-TiO₂ 化合物的比热容、熵和焓等热力学性能,模拟得到的误差范围在 5%以内。模拟结果表明,本次优化的数据库是自治和可靠的。

关键词: ZrO2-CaO-TiO2体系; 吉布斯自由能模型; 相图计算方法; 等温截面